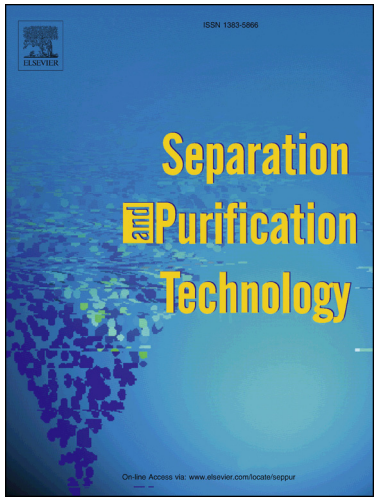

A review of principles and applications of magnetic flocculation to separate ultrafine magnetic particles

Liqun Luo, Anh V Nguyen

PII: S1383-5866(16)31055-3
DOI: http://dx.doi.org/10.1016/j.seppur.2016.07.021
Reference: SEPPUR 13138

To appear in: *Separation and Purification Technology*

Received Date: 29 October 2015
Revised Date: 26 March 2016
Accepted Date: 16 July 2016

Please cite this article as: L. Luo, A.V. Nguyen, A review of principles and applications of magnetic flocculation to separate ultrafine magnetic particles, *Separation and Purification Technology* (2016), doi: http://dx.doi.org/10.1016/j.seppur.2016.07.021

A review of principles and applications of magnetic flocculation to separate ultrafine magnetic particles

Liqun Luo[a, b*], Anh V Nguyen [b]

[a] School of Resources and Environmental Engineering, Wuhan University of Technology, Wuhan Hubei 430070, China
[b] School of Chemical Engineering, The University of Queensland, Brisbane, St Lucia Queensland 4072 QLD, Australia

**Corresponding author*. Tel: +86-15827624975; Fax: +86-27-87882128.

E-mail address: luoliqun@whut.edu.cn (L.Q. Luo)

H I G H L I G H T S

- The principles of magnetic separation have been critically reviewed;
- Both external and interparticle forces for ultrafine particles are reviewed and compared;
- Suspensions stability of the particles factors are described and analyzed;
- Various modeling of magnetic flocculation are introduced and some of the applications are illustrated.

A B S T R A C T

Magnetic separation has been used in industries to concentrate or remove magnetic minerals/particles for many years. The separation of ultrafine magnetic particles is significantly influenced by aggregation between particles due to various external and interparticle forces, such as gravity, magnetic attraction, van der Waals, electrical double-layer, hydrodynamic, and Brownian diffusion forces. This review focuses on the principles of the magnetic flocculation and separation of micrometer-sized particles in solution. Potential energies between particles are linked to the particle aggregation (i.e. stability), sedimentation and dispersion in applied magnetic fields. Prediction and control of magnetic flocculation are achieved by simulating particle motions around the surface of the magnetic separators using various mathematical models, with some large-scale applications of magnetic flocculation are being demonstrated.

Keywords: magnetic flocculation; ultrafine particles; forces; mathematical modeling

Contents

1. Introduction

Magnetic separation is typically used for concentrating magnetic materials and for removing magnetisable particles from air and liquid streams. Magnetic separation processes for ferromagnetic materials or ferrous particles have been used extensively in the past [1-3]. The use of very fine magnetic matrix elements to improve the removal of magnetic particles from suspensions has been steadily increased in recent years [4-7]. This technique has also been successfully applied in solid waste separation and recycling, ultra purification of many fine chemicals, nano and biotechnology, etc [8-13]. For instance, magnetic seeding flocculation was employed to remove arsenic by applying magnetite (Fe_3O_4) and polymeric ferric sulfate (PFS), with these two substances being separated using open or high gradient superconducting magnetic separation (OGMS or HGMS), giving rise to increase of arsenic removal from 72.5% to 90.9% when magnetite dosage increased from 25 to 300 mg/l [14].

Many of the separation techniques such as magnetic separation and flotation require liberation by fine grinding in order to increase the recovery of low grade and finely disseminated minerals. Fine particles have small attraction by magnetic force and other competing forces. Magnetic force generated by various magnetic separators, on a hematite particle, as a function of particle size is shown in Fig. 1 [15]. The low separation efficiency and recovery of ultrafine magnetic particles (< 5 μm) is mainly due to their low magnetic force and collision efficiency [16-18]. For the sake of convenience, the size classification is reproduced in Table 1. For ultrafine particles, it is theoretically and experimentally shown that magnetic separation efficiency declines significantly with decreasing particle size. Thus, many techniques have been developed to increase the effective particle size and mass, in addition to decreasing the specific surface potential energy. However, all these techniques share the same key feature that ultrafine particles should be induced to form aggregates [19]. For example, flocculation of iron hydroxide is applied to adsorb and entrap heavy metal ions dissolved in water, where superparamagnetic nanocomposite microparticles act as seeds for iron hydroxide precipitates [13]. In addition, various types of magnetic particles have been synthesized and investigated to remove magnetic particle tagged algal and microalgae from lakes based on the intrinsic paramagnetic movement [10, 20].

Magnetic flocculation of weakly magnetic materials or paramagnetic minerals, as shown in Fig. 2, has been suggested as a method to recover mineral particles of micrometer-sized or colloidal size that are usually lost in conventional separation processes [18, 21, 22]. Many researches [1, 4, 8, 23] have been concentrated on the attraction, flocculation and adherence of magnetic or weakly magnetic particles and concluded that the removal of paramagnetic particles of sizes less than approximately 40 nm was impractical. although the use of fine magnetic elements such as magnetite can enhance the performance of an high-gradient magnetic separation (HGMS) process very well in the removal of larger magnetic nanoparticles. Methods for selective enhancement of the magnetic properties of minerals include [24, 25]:

1) Selective surface decomposition of iron pentacarbonyl (Magnex process)
2) Selective wetting by magnetite laden oil (Murex process)
3) Selective co-flocculation with magnetite and
4) Selective surface adsorption of fine magnetite.

If a suspension is flocculated using a high molecular weight polymer in the presence of fine magnetite, then it is highly likely that some of the magnetite particles will become incorporated into the flocs. This aggregation can be due to either adsorption of the flocculant onto the magnetite or simple mechanical entrainment of the magnetite within the flocs. In either case the flocs are then amenable to be recovered by magnetic forces.

In the present literature, correlation coefficients or equations of theoretical predictions are reported, in addition to the highlights regarding the agreement and discrepancies between the models and the available experimental results for natural magnetic flocculation and hydrophobic-magnetic coagulation suspension of paramagnetic mineral particles such as hematite and siderite. Some models use a short-range exponential formula which was adopted to

express the hydrophobic interaction potential energy and flocculation kinetics. The surface properties of the studied particles were taken into account for the solid-liquid interfacial energies and the surface (zeta) potentials [26, 27].

Therefore, this paper critically reviews the literature on the principles of magnetic flocculation and separation of ultrafine ferrous particles as well as their application that has attracted much attention. Our particular aim is to focus on the magnetic flocculation mechanisms to improve the understanding of the magnetic separation of ultrafine particles.

2. Forces of ultrafine particles on magnetic flocculation

Magnetic flocculation separation occurs as a result of diverse colloidal forces acting on paramagnetic particles in the liquid flow field in the presence of an external field. Primary forces acting on individual particles, including external forces such as magnetic attraction, gravitational forces, and interparticle forces which act between two particles change in strength when one particle approaches to another in dilute suspensions, such as van der Waals forces, electrostatic forces, hydrodynamic resistance, and magnetic dipole attraction forces, are examined and quantified [9, 28-32]. Specifically, The separation of one material from another or the removal of magnetisable particles from streams depend upon their motion in response to the magnetic force and the other competing external forces as depicted in Fig. 3. Brownian relative diffusivity is treated separately. The scenario for magnetic flocculation study is portrayed in Fig. 4 [4, 23]. Moreover, the following theoretical analysis evaluates the interaction between two spherical paramagnetic fine particles or two magnetite ultrafine particles.

2.1 External forces

The magnitude of external forces (i.e. gravitational and magnetic attraction forces) depends on various parameters, e.g. particle size, density of the particle, magnetic susceptibility and the magnetic field. As particles with different properties travel with differing velocities in the suspension, diverse external forces are expected.

2.1.1. Gravitational force

The gravitational force, $\vec{F}_g$ acting on a particle in suspension is given by Eq. (1):

$$\vec{F}_g = \rho_p V_p \vec{g} \tag{1}$$

where ρ_p is the density of the particle, V_p is the volume of the particle, and $\vec{g}$ is the gravitational acceleration.

The buoyant force, $\vec{F}_b$, acting on a particle is given by Eq. (2):

$$\vec{F}_b = -\rho V_p \vec{g} \tag{2}$$

where ρ signifies the density of the fluid as shown in Eq. (3):

$$\vec{F}_d = -\rho C_D A_p \frac{v^2}{2} g \tag{3}$$

Where A_p is the cross-sectional area of the particle, C_D is the coefficient of drag, v, and g is the unit vector of the gravitational acceleration. Assuming laminar flow, C_D = 24/Re where Re = $2\rho va/\eta$, a is the particle radius, and η is the dynamic viscosity. Substituting these expressions for the force balance equation and assuming spherical particles allow the equation to be solved for velocity v.

2.1.2. Magnetic attraction force

The magnetic force, $\overrightarrow{F_m}$, on a particle can be given in terms of the magnetic field [16, 17] as Eq. (4):

$$\overrightarrow{F_m} = \frac{\chi}{\mu_0} VB\nabla B = \frac{4}{3}\pi a^3 \frac{\chi}{\mu_0} B\nabla B \tag{4}$$

where a is the radius of a small particle , χ is the magnetic susceptibility, μ_0 is the permeability of free space, and B is the magnitude of the magnetic induction vector $\vec{B}$. In three dimension, the magnetic induction vector, $\vec{B}$, and the magnetic-field strength vector, $\overrightarrow{H}$, are not independent but related by Eq. (5):

$$\vec{B} = \mu_0 \overrightarrow{H} \tag{5}$$

Here, H represents the local magnetic field with components in spherical coordinates given by Eqs. (6) and (7):

$$H_r = \left(H_0 + \frac{2a^3}{3r^3} M_{s,m} \right) \cos\theta \tag{6}$$

$$H_\theta = \left(H_0 + \frac{2a^3}{3r^3} M_{s,m} \right) \sin\theta \tag{7}$$

where $M_{s,m}$ is the saturated magnetization of the magnetite particle ($M_{s,m} = 4.8\times10^5 (\mathrm{A\cdot m^{-1}})$), H_0 is the magnitude of the applied magnetic field, and θ is the angle between the direction of the field (which is the same as that of the flow) and the line that connects the centers of the magnetite and nanoparticle [4, 33, 34].

The magnetic force exerted by the sphere on the small particle has radial and angular components, respectively, given by Eqs. (8) and (9).

$$F_{m2,r} = -V_2 \mu_0 (\chi_2 - \chi_m) \left(\frac{a_1 M_{s,m}}{r^4} \right) \left[2\left(H_0 + \frac{2a_1^3}{3r^3} M_{s,m} \right) \cos^2\theta + \left(-H_0 + \frac{a_1^3}{3r^3} M_{s,m} \right) \sin^2\theta \right] \tag{8}$$

$$F_{m2,\theta} = V_2 \mu_0 (\chi_2 - \chi_m) \left[-\left(H_0 + \frac{2a_1^3}{3r^3} M_{s,m} \right)^2 + \left(-H_0 + \frac{a_1^3}{3r^3} M_{s,m} \right)^2 \right] \left(\frac{\cos\theta \sin\theta}{r} \right) \tag{9}$$

For simplicity, the small particle is treated as a sphere with $V_2 = (4\pi a_2^3)/3$.

2.2 Interparticle forces

In dilute slurry, the forces occurring between two particles when one particle approaches to another, resulting in interparticle forces which play in a relatively near-field manner as compared to the external forces.

2.2.1. Van der Waals force

The van der Waals forces between particles are of fundamental importance for agglomeration processes or their structuring in suspensions [31, 32]. The coordinate system used in quantifying the interparticle forces is illustrated in Fig. 5.

The van der Waals interaction between two spheres separated by a distance l (surface-to-surface) can be derived from Hamaker's formula [4, 34, 35], given by Eq. (10):

$$\overrightarrow{F}_w = -\frac{A(16\lambda^3)}{3(a_1 + a_2)} \times \left[\frac{s}{(1+\lambda)^2 (s^2-4)^2 (s^2(1+\lambda)^2 - 4(1-\lambda)^2)^2} \right] \vec{e}_r \tag{10}$$

Where a_1 and a_2 are defined as the radii of particles 1 and 2, respectively. The larger particle is designated as 1 and the smaller particle is designated as 2 (see Fig. 5). A is the Hamaker constant, $\lambda = a_2 / a_1$ while $s = 2(l + a_1 + a_2)/(a_1 + a_2)$.

If the two spheres comprise phases 1 and 2 interacting across a macroscopic phase 3 (water), the Hamaker constant can be approximately calculated from Eq. (10):

$$A \approx \frac{3}{4}kT\left(\frac{\varepsilon_1-\varepsilon_3}{\varepsilon_1+\varepsilon_3}\right)\left(\frac{\varepsilon_2-\varepsilon_3}{\varepsilon_2+\varepsilon_3}\right)+\frac{2h\nu_e}{8\sqrt{2}}\times\frac{\left(n_1^2-n_3^2\right)\left(n_2^2-n_3^2\right)}{\left(\left(n_1^2+n_3^2\right)\left(n_2^2+n_3^2\right)\right)^{0.5}\left[\left(n_1^2+n_3^2\right)^{0.5}+\left(n_2^2+n_3^2\right)^{0.5}\right]} \tag{10}$$

Where ε_i and n_i are the dielectric constant and index of refraction of the macroscopic phase i, respectively, h is the Planck constant, and ν_e is the main electronic adsorption frequency in the UV region, typically around 3×10^{15} s^{-1}.

2.2.2. Electrical double-layer force

Electrostatic interactions among charged surfaces in electrolyte solutions determine the rate of many dynamic phenomena involving various separation procedures. An approximate expression for the electrostatic interaction was obtained between two dissimilar spheres. The expression is especially applicable when the size of the spheres is larger than the double-layer thickness and the distance between them [4, 36, 37]. Under the assumption of constant surface charge density, the electrostatic force $\vec{F}_e$ exerted by a magnetite particle on a paramagnetic nanoparticle is expressed as Eq. (11):

$$\vec{F}_e = 4\pi\varepsilon_r\varepsilon_0\kappa G_{12}\frac{e^{-h\kappa}}{1-e^{-2h\kappa}}\times((\psi_2^2+\psi_2^2)e^{-h\kappa}+2\psi_1\psi_2)\vec{e}_r \tag{11}$$

where

$$G_{12} = \frac{a_1 a_2}{2(a_1+a_2)} \tag{12}$$

$$\kappa = \left(\frac{2Ie^2}{\varepsilon_r\varepsilon_0 kT}\right)^{0.5} \tag{13}$$

and

$$I = \frac{1}{2}\sum_{i=1}^{N_i} z_i^2 n_i^b \tag{14}$$

Here, I (I=z^2n^b) is the ionic strength of the electrolyte solution and n^b is the bulk concentration of the electrolyte, ε_r and ε_0 are the relative permittivity of the medium and free space, respectively, while ψ_1 and ψ_2 are the infinite separation potentials for each particle, with the potentials being obtained from the Poisson–Boltzmann equation for single sphere under constant surface charge (σ_d) boundary condition [37, 38]. The value of σ_d represents the surface charge density which is rarely larger than 0.5 C/m^2. For simplicity, the σ_d of both particles are normally regarded as the same value.

2.2.3. Magnetic dipole force

The interaction between two magnetically susceptible particles is expressed by the interparticle magnetic potential field forces along the line of centers (see Fig. 5), given by Eqs. (15) and (16):

$$F_r^{mag} = \frac{2\pi B^2 a_1^3\chi_1 a_2^3\chi_2}{\mu_0 s^4\left(\frac{a_1+a_2}{2}\right)^4}\left\{\frac{1}{3}+\cos\left[2(\alpha-\theta)\right]\right\} \tag{15}$$

$$F_{\theta}^{mag} = -\frac{4\pi B^2 a_1^3 \chi_1 a_2^3 \chi_2}{3\mu_0 s^4 \left(\frac{a_1 + a_2}{2}\right)^4} \sin\left[2(\alpha - \theta)\right] \tag{16}$$

Where α is the angle between the direction of the vertical axis and that of the magnetic field. The angle φ defined earlier is related to α by $\varphi = |\alpha - \theta|$. It is important to note that the maximum of the tangential force is usually smaller than that of the radial force but both increase as the separation distance decreases. Also the radial force presents attractive effect when φ = 0, but becomes repulsive when φ = 90° [8, 28, 39].

The interparticle magnetic dipole force as a function of the separation distance between the two particles is shown in Fig. 6. where the magnitude of the van der Waals and that of the repulsive or attractive electrostatic forces are also presented. In addition, Fig. 6 demonstrates that the interparticle magnetic dipole force predominates over a long distance compared to the attractive van der Waals force and the attractive or repulsive electrostatic force. However, in contrast to the van der Waals and electrostatic forces which change rapidly, the interparticle magnetic dipole force reaches a plateau..

2.2.4. Hydrodynamic force

The hydrodynamic force plays a very important role when particle retention is taking place under the influence of a convective flow. In the Stokes flow regime, the modulus of the viscous or drag force, F_d, over a free-moving particle is given by Eq. (17):

$$F_d = 6\pi\eta a \left|\vec{v} - \overrightarrow{v_p}\right| \tag{17}$$

Where μ is the dynamic viscosity, $\vec{v}$ is the free stream velocity of the flow where the particle is placed, while $\overrightarrow{v_p}$ is the velocity of the particle. It is assumed that the particle velocity $\overrightarrow{v_p}$ is zero if study is concerned only with static forces between the particles.

Exact solutions for the hydrodynamic resistance to particle collision have been developed by using bispherical coordinates. Although these solutions are originally calculated for drop motion, they can be easily applied to particle motion by assigning the ratio of drop viscosity to fluid viscosity with a value of 10^3 or greater [28, 40, 41].

Hydrodynamic resistance to ax symmetric motion shows that the ax symmetric drag force, $F_{d,1}$, acting on a particle with radius a_1 moving with a velocity $\vec{v}_1$ near another particle with radius a_2 and velocity $\vec{v}_2$ is given by

$$F_{d,1} = -6\pi\eta a_1 \left(\Lambda_{11}\vec{v}_1 - \Lambda_{12}\vec{v}_2\right) \tag{18}$$

Hydrodynamic resistance to asymmetric motion developed by Zinchenko is similar to those of Haber et al [40].

$$F_{d,1} = -6\pi\eta a_1 \left(\Lambda_{11}\left(\vec{v}_1 - \vec{v}_2\right) - \Lambda_{12}\vec{v}_2\right) \tag{19}$$

where Λ_{11} and Λ_{12} are given by

$$\Lambda_{11} = \frac{\sqrt{2}\sinh(\bar{\alpha})}{3c}\sum_{n=1}^{\infty}\frac{\delta_0 + \sigma_1\delta_1 + \sigma_2\delta_2 + \sigma_1\sigma_2\delta_3}{\Delta} \tag{20}$$

and

$$\Lambda_{12} = \frac{\sqrt{2}\sinh(\bar{\alpha})}{3c}\sum_{n=1}^{\infty}\frac{\bar{\delta}_0 + \sigma_1\bar{\delta}_1 + \sigma_2\bar{\delta}_2 + \sigma_1\sigma_2\bar{\delta}_3}{\Delta} \tag{21}$$

where c, $\bar{\alpha}$, Δ and the δ and σ are coefficients derived from the geometry and fluid conditions of the situation [40, 41].

Fig. 7 shows the dimensionless hydrodynamic force as a function of the surface-to-surface separation between the paramagnetic nanoparticle and magnetite for R_p 160 and 300 nm, respectively, with superficial velocities being varying from 2 to 10 cm/min. The hydrodynamic force on the nanoparticles starts to increase significantly when the distance between the surfaces of two particles greater than about 100 nm, within this distance, the hydrodynamic force is overwhelmed by Brownian motion. However, increasing either the superficial velocity or the diameter of the paramagnetic nanoparticle has marked effects on the hydrodynamic force and can strongly affect the performance of the retention process.

2.3. Brownian forces

Particle transformation can also occur by coagulation through particle collision. The high diffusion constants of nucleation mode particles lead to rapid diffusion loss through coagulation. The large cross sections of particles larger than 10 μm lead to an appreciable growth rate through coagulation.

The relative diffusivity due to Brownian motion for two particles is expressed as Eq. (22):

$$D_{12}^{(0)} = \frac{kT(1+\lambda^{-1})}{6\pi\eta a_1} \tag{22}$$

Where, $D_{12}^{(0)}$ is Brownian relative diffusivity.

The aforementioned forces were only important if their magnitude was substantially greater than the effective Brownian force associated with random thermal motion. The forces here are evaluated in a dimensionless form relative to the Brownian force. The Péclet number (*Pe*) represents the ratio of the magnetic force to the Brownian force and is given by Eq. (23):

$$Pe = \pm\frac{a_2\left|\vec{F}_{a_1a_2}\right|}{kT} \tag{23}$$

Where a_2 is the radius of the small particle, k is the Boltzmann constant and T is the absolute temperature. The magnetic force dominates when $Pe \gg 1$. Random thermal motion overwhelms any tendency toward heteroflocculation in the opposite limit. Consequently, *Pe* can be viewed as the degree of adsorbability of the species under magnetic flocculation study [34, 42, 43].

2.4. Comparison of various forces

The magnitude of the net force is defined as the sum of the magnetic, electrostatic, and van der Waals forces, etc. The electrostatic and van der Waals forces between two spherical particles have spherical symmetry.

In general terms, interactions between mineral surfaces in aqueous media can be classified as strongly attractive, long-range repulsive referred to as dispersed, as well as weakly attractive, as shown in Fig. 8 [44].

The magnetic force acting on the paramagnetic particle is not directed along the line of particle centers. Sometimes, to simplify the comparison of force magnitudes, only those paramagnetic particle positions where the line of particle centers is aligned with the applied external field H_0 (i.e., at $\theta = 0$ or $\theta = \pi$) are considered. This allows the net force to be computed simply as a scalar sum in the model calculations. Fig. 9 contains a considerable amount of information that has been arranged for ease of comparison for different model conditions and in terms of the net dimensionless force as a function of the surface-to-surface separation between the particles.

In addition, the selective separations by magnetic flocculation are also implemented under the condition of surfactants. Hydrophobic interactions are produced due to attractive forces between hydrophobic particles. Many expressions have been proposed to describe the hydrophobic interactions between particles [25, 29].

The other important forces like hydrocarbon chain force, hydration forces and bridging forces between ultrafine particles in colloidal suspension should be achieved using reagents, such as surfactants and polymers. Most of these interactions are amenable to modification by the forces above [25].

3. Stability of magnetic flocculation suspensions

3.1. Potential energy of magnetic flocculation under various forces

The criteria of the stability of colloidal suspensions are largely governed by the interplay of repulsive and attractive forces among particles. The stability conditions can be derived from the total potential energy curve as a function of the distance between particles. When fine paramagnetic particle is exposed to an applied magnetic field *B*, the interaction of paramagnetic in magnetic flocculation processes is often expressed in the form of potential energy, depending on various forces mentioned above.

When a suspension of ultrafine particles is placed in an external uniform magnetic field, the magnetostatic (or the dipolar interaction) energy V_{Mag} between a pair of spherical particles can be written as Eqs. (24) and (25):

$$V_{Mag} = \frac{4\pi^2 B^2 a_1^3 \chi_1 a_2^3 \chi_2}{9\mu_0 \left(s\frac{a_1 + a_2}{2} \right)^3} [\overrightarrow{m_1} \bullet \overrightarrow{m_2} - 3(\overrightarrow{m_1} \bullet \vec{l})(\overrightarrow{m_2} \bullet \vec{l})\vec{l}^{-2}] \tag{24}$$

If $a_1 = a_2 = a$, then

$$V_{Mag} = \frac{16\pi^2 a^6 \chi^2 B^2}{\mu_0 l^{-3}} [\vec{m}_1 \cdot \vec{m}_2 - 3\left(\vec{m}_1 \vec{l}\right)\left(\vec{m}_2 \vec{l}\right) / \vec{l}^{\,2}] \tag{25}$$

Where, μ_0 is the magnetic permeability of vacuum, $\vec{m}$ is the magnetic moment of each particle, and l is a distance between two particles. Under certain assumptions, the expression for V_{Mag}, can be approximated:

$$V_{Mag} = \frac{4\pi^2 B^2 a_1^3 \chi_1 a_2^3 \chi_2}{9\mu_0 \left(s\frac{a_1 + a_2}{2} \right)^3} (1 - 3\cos^2 \varphi) \tag{26}$$

Where χ is the volume magnetic susceptibility of particle, and B_0 is the magnetic induction.

Electrical double layer and van der Waals interactions exist in some cases, each having their own limitations and ranges of validity. A detailed account of these expressions has been given elsewhere [45, 46]. The van der Waals interparticle force potential, V_{vdw}, was calculated by Hamaker [35] for unequal sized spheres as a function of separation

$$V_{vdW} = -\frac{A}{6}\left\{ \left[\frac{8\lambda}{\left(S^2 - 4\right)\left(1 + \lambda\right)^2} + \frac{8\lambda}{S^2\left(1 + \lambda\right)^2 - 4\left(1 - \lambda\right)^2} \right] + \ln\left[\frac{\left(S^2 - 4\right)\left(1 + \lambda\right)^2}{S^2\left(1 + \lambda\right)^2 - 4\left(1 - \lambda\right)^2} \right] \right\} \tag{27}$$

In particular, for two equal particles, i.e., $a_1 = a_2 = a$, then van der Waals attraction energy can be expressed by,

$$V_{vdW} = -\frac{A}{6}\left(\frac{2}{S^2 - 4} + \frac{2}{S^2} + \ln\frac{S^2 - 4}{S^2}\right) \tag{28}$$

Although Derjaguin's methods have been widely used to obtain double layer interaction for large values of κa (>5) at all surface potentials, it has been shown that the Derjaguin values increased with increasing distance between particles. A general limiting form of the interaction energy of two spheres at large separations ($\kappa l \gg 1$) was derived [28, 30, 46, 47].

$$V_{El} = \varepsilon\left(\frac{kT}{e}\right)^2 Y_1 Y_2 \frac{a_1 a_2 (s-2))}{r} e^{-kl} \tag{29}$$

$$Y_i = 4\tanh\left(\frac{\Phi_i}{4}\right) \tag{30}$$

$$\Phi_i = \frac{ze\Psi_{0i}}{kT} \tag{31}$$

Where Y_i (i = 1, 2) is the effective (reduced) potentials, z is the valence of the symmetric electrolyte in the solution, e is the electron charge, k is the Boltzmann constant, Ψ_{0i} refers to the particles' surface potential, and I is the ionic strength of the solution.

Theory DVLO shows that under certain assumptions, the repulsive energy of double layer can be expressed in a simple approximate form as Eq. (32):

$$V_{El} = \varepsilon a \psi_p^2 \frac{\exp(-\kappa a(s-2))}{s} \tag{32}$$

Hydrophobic–magnetic coagulation or flocculation are due to attractive forces between hydrophobic particles. Although there are uncertainty and considerable debate regarding the origin and the mechanism of the hydrophobic interactions, they are believed to arise from the perturbation of the water structure as the particles approach each other. Some researchers proposed that the hydrophobic interactions consist of two components: one long-range component which is described by an exponential force law and another arises from the association of the hydrophobic chains adsorbed on the particle surface, with the latter being held for very short particle distances $L \leq H \leq 2L$, where L is the length of the hydrocarbon chain of the surfactant [29, 44, 48]. The hydrophobic energy of interactions for two spherical particles with adsorbed layer thicknesses of δ_1 and δ_2, respectively, is expressed in the form as Eq. (33).

$$V_{Hpb} = -2\pi r \gamma_{SL} \lambda' \exp\left(\frac{h_c - h}{\lambda'}\right) \tag{33}$$

in which γ_{SL} is the solid/water interfacial energy of the spheres, h_c is the contact separation distance of the spheres (≦0.2 nm), and λ' is the empirical constant or a decay length, normally 1 nm. The greater the hydrophobicity of the spheres in water, the higher the value of (positive) γ_{SL}, and more attractive is the mutual hydrophobic interaction between the spheres [26, 49].

Therefore, by adding together the energy contributions it is possible to predict the variation in potential energy with particle separation. A net repulsive energy or a high-energy barrier will tend to prevent contact of the mineral and magnetite particles, thereby inhibiting the formation of a magnetite flocculation or coagulation. Depending on the actual particle system, special potentials might occur. If it is assumed that these energies are additive, the total potential energy of interaction is the sum of these interaction energies over all pairs of particles, which can be calculated as follows:

$$V_T = \sum V_i = \sum\left(V_{Mag} + V_{vdW} + V_{El} + V_{Hpb} + \cdots\right) \tag{34}$$

The above expressions of Eq. (34) have shown that the total energy of interaction-distance profile is uniaxial by nature whose pattern depends not only on the properties of materials involved (such as the particle size, ζ-potential of particles and Hamaker constant) but also on the process parameters (such as the composition of the electrolyte, the magnetic field strength and particle concentration), besides the hydrodynamic resistance that is taken into consideration, sometimes, involving bridging forces (V_B), hydration forces (V_{Hdn}), Hydrocarbon chain association (V_{Assoc}), etc [8, 25, 45].

The omission of the magnetic dipole energy implies that all particles considered in the flocculation system have

the same magnetic moment and dipole orientation. The behavior of suspension of paramagnetic as well as diamagnetic particles is described in Eq. (34) in an external magnetic field, and the term V_{Mag} is of the same order of magnitude as terms V_{vdW}, or V_{El} [30].The height of the potential barrier determines the stability of the suspension. In some special cases, a secondary minimum can be significantly deep to play an important role in flocculation.

3.2. Collision efficiency, collision frequency and flocculation frequency

From the curves representing the total potential energy of interaction, the criterion of the initiation of magnetic flocculation can be derived. But how quickly will flocculation take place is still an open question.

In this section, two such parameters, the collision frequency and the collision efficiency, are therefore discussed. The collision rate, J_{ij}, for a given particle will be the number of collisions it experiences per unit time. In the cases of cylindrical symmetry given in the previous section, the collision rate can be thought of as the flux of potential collision partners that move through the circle the limiting trajectory forms about the z axis.

The overall collision rate per unit volume for the two particle classes will be the collision rate for a particular particle multiplied by the concentration of that class of particles [28, 50], as indicated in Eq. (35):

$$\frac{J_{ij}}{n_i n_j} = V_{ij}^{(0)} \pi y_c^{*2} \tag{35}$$

where n_i and n_j are the concentrations of particles *i* and *j*. Note that the collision frequency without particle-particle interactions is given by Eq. (36):

$$\frac{J_{ij}^{(0)}}{n_i n_j} = V_{ij}^{(0)} (a_i + a_j)^2 \tag{36}$$

Particles not flowing around each other collide and flocculate only if they are originally on a direct collision course, much like sticky billiard balls. This collision frequency is normally taken as the reference situation with the collision efficiency, E_{ij}, defined as the ratio of the actual and reference collision frequencies followed by Eq. (37).

$$E_{ij} \equiv \frac{J_{ij}}{J_{ij}^{(0)}} = \frac{y_c^{*2}}{(a_i + a_j)^2} \tag{37}$$

Stated in a different way, the collision efficiency is the collision rate with interparticle forces divided by the collision rate without interparticle forces. If only binary particle collisions are considered and particle interactions are ignored, the binary collision frequency β_{ij} is given by Eq. (38):

$$\beta_{ij} = 4\pi D_\infty \left(a_i + a_j\right) = \frac{2}{3} \frac{kT}{\mu} \frac{\left(a_i + a_j\right)^2}{a_i a_j} \tag{38}$$

Where, D_∞ is the diffusivity of the particles in the suspension in the absence of interparticle forces.

Furthermore, the flocculation frequency F_{ij} of particles under the influence of interaction forces is defined as the product of the collision-frequency function with a collision efficiency factor E_{ij} [8, 51], as shown in Eq. (39):

$$F_{ij} = \beta_{ij} E_{ij} \tag{39}$$

Fig. 10 shows collision efficiencies of particles with various relative sizes when van der Waals and hydrodynamic forces operate, indicating thathydrodynamic forces reduce the collision efficiency of interacting particles. In addition, when the size of the particle is similar, the collision efficiency is reduced more significantly.

It is important to note that the definition of the collision efficiency factor does not limit its values between 0 and 1. For example, in the cases of a strong attractive force among the particles, E_{ij} may be greater than 1. With the above definitions and equations, the theoretical framework for a particle-particle flocculation trajectory analysis model is sufficient for useful numerical simulations.

3.3. Threshold field in magnetic flocculation

Threshold flocculating magnetic field, B_F, is an important factor at which the potential barrier between particles disappears and particles can flocculate into a potential well. Conditions of rapid flocculation into a potential well are derived in terms of threshold magnetic field as a function of particle size, magnetic susceptibility and, concentration, surface charge, etc [17, 52]. The value of magnetic field that the particles begin to flocculate is calculated based on Eq. (40):

$$B_F = \left(\frac{2kT\mu_0}{\pi^2\chi^2 a^3}\right)^{1/2} \cong \left(\frac{2kT\mu_0}{\pi^2\chi^2 a^3}\right)^{1/2} \tag{40}$$

The dependence of threshold magnetic field calculated and determined in interaction energy, on particle sizes for various minerals was given in Fig. 11, which indicates that B_F strongly depends on particle radius and on magnetic susceptibility, e.g. decreases with increased particle radius and magnetic susceptibility.

3.4. Magnetic flocculation kinetics and its stability factor

The initial stage of the flocculation process can be modeled by placing one particle at the origin of the coordinate system, and assuming that all other particles flocculate only with this central particle but not among themselves. For spherically symmetric interactions n is the particle number density which can be calculated according to Eq. (41) [2, 5],

$$n(r) = e^{-(V/k_BT)}\left(N_0 + \frac{J}{8\pi D}\int_{\infty}^{r}\frac{e^{V(x)/k_BT}}{x^2}dx\right) \tag{41}$$

where j is the particle flux using the boundary conditions Einstein's diffusion coefficient D for a single particle.

It has been shown that the stability of suspensions depends on the magnitude of the barrier and the existence depth of the secondary minimum. The number of particles to be halved is given by Eq. (42) [17, 30].

$$t_{1/2} = \frac{3\eta W}{4kTN_0} \tag{42}$$

Where t is the time, η is the viscosity of the medium while N_0 is the initial concentration of the particles. The stability ratio W is calculated according to Eq. (44):

$$J = \frac{8\pi DN_0 d}{W} \tag{43}$$

$$W = 2\int_2^{\infty}\frac{V_T}{e^{kT}}\bullet\frac{ds}{s^2} \tag{44}$$

The stability factor, W depends on the magnitude of the potential energy of interaction. The different curves correspond to different values of V_{R0} $\left\{V_{R\mathbf{0}} = \left[(\pi\varepsilon_{\mathbf{0}}\varepsilon_r d\psi_{\mathbf{0}}^2)/k_BT\right]e^{\kappa d}\right\}$, which determines the zero-field stability [2, 5]. Consequently, the factor of stability can be used to determine the degree of colloid stability of a given system.

Representative results are given in Fig. 12 for κd =1 in terms of the stability factor W as a function of β (W = 3.014678 $\times\beta^{-2/3}$). The dimensionless parameter β is showed in Eq. (45).

$$\beta = \chi Bd^{3/2}\sqrt{\frac{\sqrt{3}\pi}{144\mu_0 k_B T}} = 2728\chi Bd^{3/2} \tag{45}$$

For small values of β the effect of the magnetic interaction is negligible, as can be expected when $|V_M/k_BT| \ll 1$. For large values of β however, the magnetic interaction is dominant.

4. Multi-method modeling of magnetic flocculation particles

Modeling analysis and evaluation is based on various forces, potential energy interaction and collision relationship of the interparticles. The mathematical express of flocculation is based on the process considering that the destabilized suspended particles are aggregated through two steps: transport and attachment. The rate of flocculation expressed mathematically as successful rate of collision between particles with sizes of *i* and *j*. Nearly all flocculation models are based upon Eq. (47) [53].

$$rate\ of\ \ flocculation = \alpha\beta(i,j)n_i n_j \tag{47}$$

There are various flocculation processes models such as Smoluchowski's and Fucks's models, rectilinear and curvilinear models. The more recent microscopic approach based on characterization of the system through determination of the fractal dimension as a function of time offers the opportunity of a simpler yet more representative modeling [54-56].

4.1. Fundamental theory of magnetic flocculation modeling

Pair-Dipole Model. If the magnetite particles within colloidal suspension are very small and randomly distributed, the composite particles are treated as single-domain structure and the dipole model is applicable. Magnetic dipoles are attractive along the field direction and repulsive to the field direction. Hence, the interacting colloidal particles form chain aggregates that are aligned along the field direction. The magnetic-dipole interaction is determined for an isolated pair of particles and is referred to as the pair-dipole model [57, 58].

Chain-Dipole Model. Particles trapped in a chain also experience magnetic induction from other particles in the same chain, as well as from the externally applied magnetic field. The magnetic potential energy between any two particles in a chain was referred to as the chain-dipole model and was calculated in modeling.Therefore, the magnetic induction at particle *i* ($\boldsymbol{B}_i$) in a chain of *N* particles is the summation of the externally applied magnetic induction at particle *i* ($\boldsymbol{B}$) and the induction from other particles in the chain ($\boldsymbol{B}_{ij}$). The total potentials between the two central particles in a chain are determined whether the aggregation is in primary or secondary minimum.

4.2. Univariate population-balance (PB) method

Simulation of magnetic flocculation behaviour of fine minerals was described by direct computation of the Brownian, van der Waals, Born, electrical double layer and magnetic forces acting on each particle [17, 45]. An electrolyte of distilled water with a low conductivity had been considered employing comparable conditions to those reported by Svoboda [30]. Fig. 13 shows a typical plot of total interaction energy of two hematite particles with a diameter of 5 μm under several magnetic fields, e.g. the potential barrier prevents particles from flocculating into the primary minimum when *B*=0.01T, while when *B*=0.02T the interaction energy was purely attractive, and particles can coagulate into the potential well. Such a magnetic field was considered as a threshold field for which the flocculation begins.

4.3. Bivariate population-balance (PB) method

Kinetics of heterogeneous magnetic flocculation using a bivariate population-balance (PB) equation had been focused on aspects: (i) to predict the flocculation rate of mixed paramagnetic particles in a magnetic field and (ii) to use the flocculation rate for the prediction of transient floc size and floc concentration in terms of various types of the initially present particles [39, 59]. The discrete bivariate PB equation for a batch system is written as Eq. (48):

$$\frac{dn_{ij}}{dt} = \frac{1}{2}\sum_{l=1}^{i-1}\sum_{m=1}^{j} n_{lm} n_{(i-l)(j-m)} F_{lm,(i-1)(j-m)} - \sum_{l=1}^{N_s - i}\sum_{m=1}^{l+N_c^l-1} n_{ij} n_{lm} F_{ij,lm} \quad (48)$$

Where n_{ij} (m^{-3}) is the number of particles with a size of *i* and a concentration of *j* (class *ij)*; *t* is the time; $F_{ij,lm}$ (m^3s^{-1}) is the flocculation frequency of particles in class *ij* with particles in class *lm; N_s* and N_c^l are the total numbers of particle and initial concentration, respectively. The factor 1/2 is required to eliminate double summation over the same size-concentration. The term on the left side of Eq. (48) is the accumulation term for particles with a size of *i* and a concentration of *j*, the first term on the right side is a source term due to flocculation of smaller particles, and the second term on the right side is a loss term due to flocculation to larger particles (flocs). An efficient discretization of magnetic susceptibility and size is shown in Fig. 14.

As most complex processes involving changes in the size of particulate components, modeling procedures based on stochastic approaches are generally far superior to deterministic models. The commonly used computer stochastic simulation techniques can be classified into Monte Carlo (MC), Molecular Dynamics (MD) and Brownian Dynamics (BD) methods. Since the MC [45, 60] is now a well-established and standard technique in the field of computer simulations, it suffices to describe the magnetic flocculation procedure very well, for instance, hematite particles were confined to a cubic simulation box of side *L* with periodical boundary conditions. During each simulation cycle, every particle in the simulation box is picked up in turn and moved randomly, then the change in the configuration energy ΔV due to the movement of a particle is calculated.

The results of discrete bivariate PB equation showed the effect of particle size and magnetic susceptibility on the bivariate (volume/magnetic susceptibility) density as a function of time, i.e. from initial condition to more than 10 min of flocculation. These results can be used to determine the degree of heterogeneous flocculation that is important in the separation of particles of different magnetic susceptibility.

4.4. Fractal dimension method

Dynamic methods have been adopted to simulation systems for macroscopic and or colloidal particles. The dynamics of aggregation or flocculation is characterized in terms of mean particle size, fractal dimensions, distribution of orientations and radial distribution function for different-sized particles. In flocculation kinetics models conventional methods are often based on discretisation of global population balance methods, and it is usually assumed that spherical particles collide and form spherical aggregates. Real aggregates or flocs, however, are of irregular shapes and can be considered as fractal objects. From small to large diameters, the distribution of orientations gradually approaches the orientation of the magnetic field, the larger particles forming chain-like clusters, the smaller ones forming clusters with branched and looped shapes. The structure of fractal objects can be described by a fractal dimension number that plays an important role in magnetic aggregation kinetics [57, 61, 62]. Meantime, there have been many methods to describe the geometrical structure of a floc. Fractals can be defined as disordered systems with a nonintegral dimension. Fractal dimensions may be defined in linear, planar or volumetric terms, resulting in so-called one-, two- or three-dimensional values, respectively [62-64].

A fractal dimension, D_F, which is described as the packing of the particles forming the aggregate, varies from 1 to 3. The higher the value of D_F, the more densely packed the aggregates, e.g. a fractal dimensions of 3 indicates a solid spherical structure. Fractal aggregates have two important properties viz. self-similarity and power law behavior [61, 65].

The relation between the radius of gyration, R_g and the number of primary particles, n_p, follow the power-law of Eq. (49),

$$R_g \propto n_p^{1/D} \quad (49)$$

Where *D* is fractal dimensionality. The radius of gyration of the maximum chain, R_G, which can be obtained by cutting off the portion of branches (Fig. 16).

The growth mechanism of the linear chain consists of the accumulation of isolated particles or small clusters onto existing chains, which are all moving at different speeds, during aggregation of paramagnetic particles. The chain length increases linearly and has a growth rate that increases as a power law with the shear [66].

As far as the two-dimensional fractal dimension, D_2, is defined in terms of the relationship between the increase in radius and the corresponding increase in mass contained within the circle or, in geometrical terms (Eq. (50)),

$$A_g \propto R_p^{D_2} \tag{50}$$

Where A_g is the sum of areas of all primary particles contained within a circle of radius R_p. Thus, D_2 may be found as the slope of a plot of log A versus log R_p. Fig. 17 shows the planar aggregates, where each solid circle represents the mass of a primary particle, it is clear that circles of different radii drawn about the center of the aggregate enclose different masses.

Now with the light scattering method widely being used to determine the fractal dimension, results from this simulation will be readily used once the relationship between fractal dimension and permeability is developed. The mass fractal dimension of the flocs is obtained from the settling rate and size data in the settling experiments and through logarithmic correlation between the mass and the size of the flocs, considering spherical geometry [67, 68].

For magnetic flocculation systems the mean chain length L_m defined by Williams [45] is the best single quantity to describe the chain flocs. The chain length L_c as the maximum length of the floc measured in Y-axis (i.e., the direction of the magnetic field) while the average value of the maximum lengths measured in X- and Z-axes gave the chain thickness T_c. The mean chain length L_m and mean chain thickness T_m (R_m=L_m/T_m) are obtained by averaging the chain length and thickness over all flocs in the simulation box. The results illustrate that the MC simulation method can correctly predict the trend of changes in the mean chain length as a function of process parameters (magnetic field B, particle radius a and particle volume fraction γ) and the floc size distribution function [45]. However, exploration of the flocculation behaviour is sensitive to particle charge, ionic composition of electrolyte, particle size, particle concentration and magnetic field strength and orientation. The limitations lie in additional hydrodynamic effects and the walls of a process vessel or pipe, compared to a realistic simulation.

5. Applications and aspects of magnetic flocculation

Magnetic flocculation separation is one of the cornerstones for fine material manipulation and available for applications in various industries. Magnetic flocculation is expected to create cluster of particles several times greater than individual particles, and then these flocs can be easily recovered in a high-gradient magnetic separator. Applications of magnetic flocculation are used not only for fine mineral and material separation, but also the following aspects:

(a) increasing solid setting rate and reducing the size and costs of dewatering equipments;
(b) producing and maintenaning clean water, reducing pollution problems;
(c) increasing the difference between flocculated magnetite and unflocculated gangue slime;
(d) improving filtering rate of ferromagnetic products and reducing blinding of filter cloth;
(e) reducing the amount of flocculating reagents added.

This method has a number of advantages, for instance, no chemical agents required, low operating costs less ecological problems and flocculation time, rapid separation, space saving, etc. Other advantages are electrical and mechanical energy savings, simple operation and design, sedimentation acceleration and high-rate solid–liquid separation [69, 70]. and is potential to be utilized in various industries ranging from mine exploitation, steel producing industry and waste water treatment plants to food industry and biotechnological application in the future [9, 17].

5.1. Floc size measurement and density analysis

Floc size distributions are determined using a Malvern particle size analyzer (Malvern Instruments, Type 2600, England). The output from the instrument is interfaced directly to a computer, which performs the necessary calculations [71]. After experimental results show that the size distribution of flocs, the computer can report particle size distributions which are transformed to a distribution in terms of number percentages for use in the lumped model. Information on the true size of the aggregate can be obtained by the small angle light scattering technique (SALLS), or more accurately, from image analysis done using the Transmission Electron Microscope [67].

A developed instrument called the Floc Density Analyzer was used to measure the density, size and shape of hematite flocs. The instrument uses high magnification optics linked with a video camera to view flocs settling in a specially designed cell. The cell design and floc concentration is such that flocs settle under their own weight, without any disturbance from liquid convection currents or interactions with each other. Examination of the video images allows measurement of floc sizes, shapes and settling rates via a monitor/video recorder calibrated in units of length. The floc sizes and settling rates are simultaneously transferred to a computer. The floc size (diameter) is calculated from the maximum horizontal and vertical dimensions of the floc in terms of the diameter of a sphere with a settling velocity equivalent to the floc. The floc density is then calculated using Stokes' Law [72].

Mutual hindrance among highly concentrated particles in sedimentation leads to velocities lower than those calculated by Stokes Law, which could be differentiated by the three regimes of Fig 17: "swarm sedimentation", "zone sedimentation" and "compression" as particle concentration increases. Later, the sedimentation behaviour of the floc was treated by Scott in terms of a flocculation number k and the actual solids volume concentration c_v [70, 73].

When extrapolating the linear zone sedimentation region towards a concentration of 0 and towards higher concentrations, the intersection with the y-axis is the single floc settling rate $u_{fl,St}$ to the 1/4.65 power and the intersection with the x-axis is the flocculation number k_F. From those two characteristic values, $u_{fl,St}$ and k_F which may be obtained by fitting experiment data, the floc density ρ_F and floc size d_F can be calculated:

$$\rho_F = \frac{\rho_s - \rho_l}{k_F} + \rho_l \tag{51}$$

$$d_F = \sqrt{\frac{18\eta\mu_{fl,St}}{(\rho_F - \rho_l)g}} \tag{52}$$

The radio-frequency method can be used to study processes of sedimentation and flocculation of various minerals having both low and high solid contents in pulps, is relatively easy to automate, and allows use of computer for data analysis right during the measurement [74]. The data on the change in the oscillatory circuit frequency f referred to m = 1 g of various minerals are cited in Table 2. Automation of flocculation analysis by using a torsion balance that allows monitoring of the settled mass of the material right in the lower part of the cylinder containing water for different lengths of time or by using a photoelectric colorimeter is difficult. The rate of the flocculation processes is measured from the rate of sedimentation in the lower part of the cylinder.

Recent studies have shown that a focused beam reflectance-measuring probe (FBRM) was used to get information about the average chord of the aggregates and the number of counts, that light diffraction scattering (LDS) was a useful technique to monitor the dynamics of flocculation and to evaluate the influence of the flocculant characteristics and dosage [75, 76]. LDS not only allows the determination of the aggregate mean size and size distribution, but also gives the mass fractal dimension of the flocs.

The US patent relates to a nuclear magnetic resonance detected and monitored the flocculation kinetics of high molecular weight fractions of a complex fluid by the relaxation signals and the flocculation rate [77]. Moreover, In situ observation methods and experimental results were presented quartz-magnetite pearl chain during

magnetite coagulates by Helmholtz coils for magnetic measurements [78, 79]. In-situ estimations of the density and porosity of flocs of varying sizes in a submarine canyon [80], floc density and porosity were estimated directly from floc volume and primary particle mass by measure suspended particle volume and mass concentrations of 32 and 3 size-classes, respectively. The porosity of a floc particle is the ratio of the volume of the interstitial pore space to that of the floc particle.

5.2. Eriez permanent magnetic flocculators

In spite of magnetic flocculation of either strongly magnetic materials or weakly magnetic minerals, the effects due to such variables like magnetic field strength, particles size and distribution, content of solids, velocities of flow and degree of stirring are investigated in commercial and industrial applications. For example, hematite or siderite particles smaller than that 10 μm can be flocculated at a reasonably low magnetic field, while large particles will be unaffected as indicated in Table 3. It means that it is possible to to obtain homogenous slurry with a -10 μm fraction. As the initial concentration of relatively large particles is so low, longer retention time in the magnetic system is required for efficient flocculation to occur, or a magnetic field greater than the threshold flocculating magnetic field is required [52].

Conventional methods for cleaning steel mill waste and process waters include sedimentation, flocculation_and fixed bed filtration. Such approaches require either large areas for settling tanks and clarifiers or expensive and short-lived filter systems [9, 81]. Magnetic flocculation and separation has emerged as an ideal solution to treat industry wastewater, and it has offered great time, space and cost savings [82, 83].

Eriez permanent magnetic flocculators, aiding in the separation of magnetic particles from liquids and slurries, are used widely in the iron and coal mining industries to speed settling of fine magnetic particles in ore slurries and heavy media slurries, as well as some other industries for agglomerating fine magnetic contaminants in quench water, cooling oils, etc. Compact, powerful units having Erium permanent magnets speed up settling of magnetic solids from slurries and liquids for easier recovery and separation. Magnetic flocculation requires only split-second exposure to magnetic flux generated by the permanent magnets on top and bottom. An Eriez flocculator magnet installed at a large steel plant (Fig. 18) indicates that magnetic flocculation reduced ferrous solids in overflow from 600 parts per million to as low as 40 parts per million. Further studies indicate that reduction in suspended solids contents of treated waste waters is typically greater than 90% and often exceeds 99%. A magnetic flocculator therefore can be adapted to many chemical flocculation installations with the effect of reducing operating costs.

5.3. Flocs generator reactor

The success application of permanent magnet roll separators is a result of two factors: the availability of a large variety of magnet grades and sizes with low cost, the availability of electromagnetic modeling software that allows the optimization of the design [15, 84]. However, further investigations are needed to examine the relationship between the measurements of composite of the real ultrafine particles and the magnetic flocculation recovery in other industrial processing systems [10].

Flocs generator reactor (FGR) has a good potential as an in-line flocculation (or flotation) separator device in applications requiring high solid–liquid separation rate in water and wastewater treatment [68, 69]. A compact flocculation system provides high process efficiency and high loading capacity before the solid–liquid separation, where the flocculation of particles is assisted by the kinetic energy transfer from the hydraulic flow through the reactor. In this system, not only the flocculation is favored (higher turbulence) but also the entrainment and/or entrapment of the air bubbles inside the flocs leading to formation of big aerated units (Fig. 19). The hydraulic performance and advantages of the FGR, besides reducing considerably the foot print area (by enrolling its overall length), forms large and dense flocs which promptly settle, and avoids electrical and mechanical energy consumption. Therefore, the applications of magnetic flocculation for ultrafine magnetic particle separation will

increase considerably since such a reactor holds a great potential in the development of eco-based economies.

5.4. Shearing magnetic floc in a water treatment

Fig. 20 shows a systematicl device to utilize a magnetic floc and separation technique in a batch treatment process to treat wastewater [85, 86]. This system includes a tank, a mixing device, a horizontal shearing device, rotatable magnets or magnetic drum, and scraper. The horizontally extended shear tank have a plurality of blades space along a horizontally extending elongated shaft located in the tank to stir the flocs. The magnetic flocs settle in a lower portion of the tank while purified water is decanted from the upper port of the tank. A stirring device shears the magnetic floc producing magnetic seed and sludge. A magnetic field retains the magnetic seed while the sludge is discharge from the tank as a batch process, with the retained magnetic seed being reused in subsequent batches of water treatment [85], producing a method of collecting swath magnetic floc, transferring the floc to the shear tank, magnetic seed from the floc to produce a slurry swath, and transferring the slurry swath to a magnetic device to separate the magnetic seed for recycling in continuous flow application [86].

The sizes of magnetic particles normally ranges from 30 to 50 microns can be used as seed to bind or sorbing pollutant particles which can be removed subsequently. Furthermore, some extreme example with the application of magnetic seed size down to approximately 20 nanometres can be used to remove nano pollutant particles. These process is typically done at a magnetic seed concentration of approximately 0.5 to 1%, some cases may up to about 3~5% [85, 86].

6. Conclusions

Mineral processing industry faces many challenges and opportunities for continuous economic growth in the 21st century. Magnetic flocculation and separation processes to separate ultrafine ferrous particles are being more promising due to less operating costs and ecological problems, compared to conventional methods. The principles and applications of magnetic flocculation of ultrafine ferrous particles are critically reviewed, specifically both theoretical and the experimental work regarding various forces have been discussed for the interactions relevant to the separation of particles by magnetic flocculation for a range of mineral systems and conditions. The experimental investigations and mathematical models and stability factors in magnetic flocculation are also critically reviewed. According to the previous studies, these parameters are strongly affected by the physical properties of magnetic susceptibility, particle size and distributions, colloidal suspension chemistry. This review has discussed and expected the applications of magnetic flocculation in mineral and other industrial processes. Based on the promising characteristics of magnetic flocculation, the authors believe that series of devices and flowsheets will be proposed and developed in the near future for the designation of appropriate instruments which could further improve the applications of magnetic flocculation in various industries.

Acknowledgments

The authors gratefully acknowledge the financial support from the Chinese Government for the CSC (China Scholarship Council), and the School of Chemical Engineering at The University of Queensland for the intellectual condition, environment and support.

References

[1] A.D. Ebner, J.A. Ritter, H.J. Ploehn, R.L. Kochen, J.D. Navratil, New magnetic field-enhanced process for the treatment of aqueous wastes, Separation science and technology, 34 (1999) 1277-1300.

[2] J. Janssen, J. Baltussen, A.P. Gelder, J. Perenboom, Kinetics of magnetic flocculation. I. Flocculation of colloidal particles, Journal of Physics D: Applied Physics, 23 (1990) 1447.

[3] R.H. Perry, D.W. Green, J.O. Maloney, Perry's chemical engineers' handbook, (1984).

[4] A.D. Ebner, J.A. Ritter, H.J. Ploehn, Magnetic hetero-flocculation of paramagnetic colloidal particles, Journal of colloid and interface science, 225 (2000) 39-46.

[5] J. Janssen, J. Baltussen, A. Gelder, J. Perenboom, Kinetics of magnetic flocculation. II. Flocculation of coarse particles, Journal of Physics D: Applied Physics, 23 (1990) 1455.

[6] Y. Li, B. Zhou, F. Xu, H. Jiang, W. Zhang, The advantages of a superconducting magnetic intensity greater than 1 T for phosphate–ferric flocs separation in HGMS, Separation and Purification Technology, 141 (2015) 331-338.

[7] M. Omran, T. Fabritius, A.M. Elmahdy, N.A. Abdel-Khalek, M. El-Aref, A.E.-H. Elmanawi, Effect of microwave pre-treatment on the magnetic properties of iron ore and its implications on magnetic separation, Separation and Purification Technology, 136 (2014) 223-232.

[8] C. Tsouris, T. Scott, Flocculation of paramagnetic particles in a magnetic field, Journal of colloid and interface science, 171 (1995) 319-330.

[9] C.T. Yavuz, A. Prakash, J. Mayo, V.L. Colvin, Magnetic separations: From steel plants to biotechnology, Chemical Engineering Science, 64 (2009) 2510-2521.

[10] S.-K. Wang, A.R. Stiles, C. Guo, C.-Z. Liu, Harvesting microalgae by magnetic separation: A review, Algal Research, 9 (2015) 178-185.

[11] K. Barani, S.M.J. Koleini, B. Rezaei, Magnetic properties of an iron ore sample after microwave heating, Separation and Purification Technology, 76 (2011) 331-336.

[12] P. Fraga García, M. Brammen, M. Wolf, S. Reinlein, M. Freiherr von Roman, S. Berensmeier, High-gradient magnetic separation for technical scale protein recovery using low cost magnetic nanoparticles, Separation and Purification Technology, 150 (2015) 29-36.

[13] K. Mandel, F. Hutter, C. Gellermann, G. Sextl, Reusable superparamagnetic nanocomposite particles for magnetic separation of iron hydroxide precipitates to remove and recover heavy metal ions from aqueous solutions, Separation and Purification Technology, 109 (2013) 144-147.

[14] Y. Li, J. Wang, Y. Zhao, Z. Luan, Research on magnetic seeding flocculation for arsenic removal by superconducting magnetic separation, Separation & Purification Technology, 73 (2010) 264-270.

[15] J. Svoboda, T. Fujita, Recent developments in magnetic methods of material separation, Minerals Engineering, 16 (2003) 785-792.

[16] T. Miettinen, J. Ralston, D. Fornasiero, The limits of fine particle flotation, Minerals Engineering, 23 (2010) 420-437.

[17] J. Svoboda, Magnetic methods for the treatment of minerals, Elsevier Science Publishers, P. O. Box 330, 1000 AH Amsterdam, The Netherlands, 1987., (1987).

[18] R. Sivamohan, The problem of recovering very fine particles in mineral processing--A review, International Journal of Mineral Processing, 28 (1990) 247-288.

[19] Y. Wang, E. Forssberg, R.J. Pugh, S. Elming, Magnetic aggregation in dispersions of mineral ultrafines, Journal of dispersion science and technology, 16 (1995) 137-154.

[20] Z. Yuan, W. Liang, L. Liu, F. Li, Q. Fan, X. Sun, Harvesting Chlorella vulgaris by magnetic flocculation using Fe 3 O 4 coating with polyaluminium chloride and polyacrylamide, Bioresource Technology, 198 (2015) 789-796.

[21] J. Svoboda, Magnetic techniques for the treatment of materials, Kluwer Academic Pub, 2004.

[22] L. Luo, J. Zhang, Y. Yu, Recovering limonite from Australia iron ores by flocculation-high intensity magnetic separation, Journal of Central South University of Technology, 12 (2005) 682-687.

[23] R.L. Kochen, J.D. Navratil, Removal of radioactive materials and heavy metals from water using magnetic resin, in, Google Patents, 1997.

[24] P. Parsonage, Selective magnetic coating for mineral separation, Trans. Inst. Min. Metall,(Sect. C: Mineral Process. Extr. Metal.), 93 (1984) C37-44.

[25] P. Parsonage, Principles of mineral separation by selective magnetic coating, International Journal of Mineral Processing, 24 (1988) 269-293.

[26] J. Škvarla, F. Zelenak, Magnetic-hydrophobic coagulation of paramagnetic minerals: a correlation of theory with experiments, International Journal of Mineral Processing, 68 (2003) 17-36.

[27] J. Padding, A. Louis, Hydrodynamic interactions and Brownian forces in colloidal suspensions: Coarse-graining over time and length scales, Physical Review E, 74 (2006) 031402.

[28] S. Yiacoumi, D.A. Rountree, C. Tsouris, Mechanism of particle flocculation by magnetic seeding, Journal of colloid and interface science, 184 (1996) 477-488.

[29] G.N. Anastassakis, Separation of fine mineral particles by selective magnetic coating, Journal of colloid and interface science, 256 (2002) 114-120.

[30] J. Svoboda, Magnetic flocculation and treatment of fine weakly magnetic minerals, Magnetics, IEEE Transactions on, 18 (1982) 796-801.

[31] F. Babick, van-der-Waals interaction between two fractal aggregates, Advanced Powder Technology, 22 (2010) 220-225.

[32] F. Babick, K. Schi, M. Stintz, van-der-Waals interaction between two fractal aggregates, Advanced Powder Technology, 22 (2011) 220-225.

[33] D. Bagster, The calculation of force on a weakly magnetic particle in a magnetic field, International Journal of Mineral Processing, 20 (1987) 1-15.

[34] A. Ebner, J. Ritter, H. Ploehn, Feasibility and limitations of nanolevel high gradient magnetic separation, Separation and purification technology, 11 (1997) 199-210.

[35] H. Hamaker, The London--van der Waals attraction between spherical particles, physica, 4 (1937) 1058-1072.

[36] P. Warszyski, Z. Adamczyk, Calculations of double-layer electrostatic interactions for the sphere/plane geometry, Journal of colloid and interface science, 187 (1997) 283-295.

[37] Z. Adamczyk, Particle adsorption and deposition: role of electrostatic interactions, Advances in colloid and interface science, 100 (2003) 267-347.

[38] H. Ohshima, T.W. Healy, L.R. White, Accurate analytic expressions for the surface charge density/surface potential relationship and double-layer potential distribution for a spherical colloidal particle, Journal of colloid and interface science, 90 (1982) 17-26.

[39] C. Tsouris, S. Yiacoumi, Particle flocculation and filtration by high-gradient magnetic fields, Separation science and technology, 32 (1997) 599-616.

[40] S. Haber, G. Hetsroni, A. Solan, On the low Reynolds number motion of two droplets, International Journal of Multiphase Flow, 1 (1973) 57-71.

[41] A. Zinchenko, The slow asymmetric motion of two drops in a viscous medium* 1, Journal of Applied Mathematics and Mechanics, 44 (1980) 30-37.

[42] T. Cosgrove, Colloid science: principles, methods and applications, Wiley-Blackwell, 2010.

[43] R.H. Davis, The rate of coagulation of a dilute polydisperse system of sedimenting spheres, Journal of Fluid Mechanics, 145 (1984) 179-199.

[44] S.B. Johnson, G.V. Franks, P.J. Scales, D.V. Boger, T.W. Healy, Surface chemistry-rheology relationships in concentrated mineral suspensions, International Journal of Mineral Processing, 58 (2000) 267-304.

[45] R. Williams, X. Jia, Simulation of magnetic flocculation behaviour of fine minerals, International Journal of Mineral Processing, 32 (1991) 175-191.

[46] X. Jia, R. Williams, Particle deposition at a charged solid/liquid interface, Chemical Engineering Communications, 91 (1990) 127-198.

[47] A.V. Nguyen, H.J. Schulze, Colloidal science of flotation, CRC, 2004.

[48] Q. Liu, F.J. Friedlaender, Fine particle processing by magnetic carrier methods, Minerals Engineering, 7 (1994) 449-463.

[49] D. Li, A. Neumann, Equation of state for interfacial tensions of solid-liquid systems, Advances in colloid and interface science, 39 (1992) 299-345.

[50] X. Zhang, R.H. Davis, Rate of collisions due to Brownian or gravitational motion of small drops, Journal of Fluid Mechanics, 230 (1991) 479-504.

[51] I.A. Valioulis, E. John List, Collision efficiencies of diffusing spherical particles: hydrodynamic, van der waals and electrostatic forces, Advances in colloid and interface science, 20 (1984) 1-20.

[52] J. Svoboda, A theoretical approach to the magnetic flocculation of weakly magnetic minerals, International Journal of Mineral Processing, 8 (1981) 377-390.

[53] D. Thomas, S. Judd, N. Fawcett, Flocculation modelling: A review, Water Research, 33 (1999) 1579-1592.

[54] P.T. Spicer, S.E. Pratsinis, Coagulation and fragmentation: Universal steady-state particle-size distribution, AIChE Journal, 42 (1996) 1612-1620.

[55] D.H. Li, J. Ganczarczyk, Fractal geometry of particle aggregates generated in water and wastewater treatment processes, Environmental science & technology, 23 (1989) 1385-1389.

[56] S. Peng, R. Williams, Control and optimisation of mineral flocculation and transport processes using on-line particle size analysis, Minerals Engineering, 6 (1993) 133-153.

[57] C.J. Chin, S. Yiacoumi, C. Tsouris, Probing DLVO forces using interparticle magnetic forces: Transition from secondary-minimum to primary-minimum aggregation, Langmuir, 17 (2001) 6065-6071.

[58] H. Zhang, M. Widom, Field-induced forces in colloidal particle chains, Physical Review E, 51 (1995) 2099.

[59] C. Tsouris, S. Yiacoumi, T. Scott, Kinetics of heterogeneous magnetic flocculation using a bivariate population-balance equation, Chemical Engineering Communications, 137 (1995) 147-159.

[60] N. Metropolis, A.W. Rosenbluth, M.N. Rosenbluth, A.H. Teller, E. Teller, Equation of State by Fast Computing Machines, Journal of Chemical Physics, 21 (1953) 1087--1092.

[61] C.J. Chin, S.C. Lu, S. Yiacoumi, C. Tsouris, Fractal dimension of particle aggregates in magnetic fields, Separation science and technology, 39 (2004) 2839-2862.

[62] X. Li, K. Yao, Z. Liu, Cluster Moving Monte Carlo Simulation of Nano-Sized Magnetic Particle Aggregation in AN Applied Magnetic Field, International Journal of Modern Physics B, 23 (2009) 5307-5323.

[63] Y. Adachi, S. Ooi, Geometrical structure of a floc, Journal of colloid and interface science, 135 (1990) 374-384.

[64] R.K. Chakraborti, K.H. Gardner, J.F. Atkinson, J.E. Van Benschoten, Changes in fractal dimension during aggregation, Water Research, 37 (2003) 873-883.

[65] P. Tang, J. Greenwood, J. Raper, A model to describe the settling behavior of fractal aggregates, Journal of colloid and interface science, 247 (2002) 210-219.

[66] E. Brunet, G. Degre, F. Okkels, P. Tabeling, Aggregation of paramagnetic particles in the presence of a hydrodynamic shear, Journal of colloid and interface science, 282 (2005) 58-68.

[67] P. Tang, J. Raper, Modelling the settling behaviour of fractal aggregates-a review, Powder technology, 123 (2002) 114-125.

[68] E. Carissimi, J. Rubio, The flocs generator reactor-FGR: a new basis for flocculation and solid-liquid separation, International Journal of Mineral Processing, 75 (2005) 237-247.

[69] E. Carissimi, J. Miller, J. Rubio, Characterization of the high kinetic energy dissipation of the Flocs Generator Reactor (FGR), International Journal of Mineral Processing, 85 (2007) 41-49.

[70] M. Stolarski, C. Eichholz, B. Fuchs, H. Nirschl, Sedimentation acceleration of remanent iron oxide by magnetic flocculation, China Particuology, 5 (2007) 145-150.

[71] D. Patil, J. Andrews, P. Uhlherr, Shear flocculation--kinetics of floc coalescence and breakage, International Journal of Mineral Processing, 61 (2001) 171-188.

[72] P. Weissenborn, L. Warren, J. Dunn, Selective flocculation of ultrafine iron ore 2. Mechanism of selective flocculation, Colloids and Surfaces A: Physicochemical and Engineering Aspects, 99 (1995) 29-43.

[73] K.J. Scott, Theory of thickening: factors affecting settling rate of solids in flocculated pulps, Trans. Inst. Min. Met, 77 (1968) C85-C97.

[74] A. Zvegintsev, G. Barinov, K. Yakubailik, Investigation into processes of flocculation of finely divided minerals by radio-frequency method, Journal of Mining Science, 33 (1997) 176-178.

[75] A. Blanco, E. Fuente, C. Negro, J. Tijero, Flocculation monitoring: focused beam reflectance measurement as a measurement tool, The Canadian Journal of Chemical Engineering, 80 (2002) 1-7.

[76] M. Rasteiro, F. Garcia, P. Ferreira, A. Blanco, C. Negro, E. Antunes, The use of LDS as a tool to evaluate flocculation mechanisms, Chemical Engineering and Processing: Process Intensification, 47 (2008) 1323-1332.

[77] J. Cohen Addad, M. Fleury, Nuclear magnetic resonance method of detecting and monitoring the flocculation kinetics of heavy fractions of complex fluid, in, US Patent App. 20,050/083,052, 2003.

[78] S. Trout, Use of Helmholtz coils for magnetic measurements, Magnetics, IEEE Transactions on, 24 (1988) 2108-2111.

[79] H.A. Garcia-Martinez, S. Song, A. Lopez-Valdivieso, In situ observation of quartz particles entrained into magnetite coagulates in a uniform magnetic field, Minerals Engineering, 24 (2011) 963-966.

[80] R.T. Hsu, J.T. Liu, In-situ estimations of the density and porosity of flocs of varying sizes in a submarine canyon, Marine Geology, 276 (2010) 105-109.

[81] S.L. Cort, Magnetic separation and seeding to improve ballasted clarification of water, in, US, 2010.

[82] J. Oberteuffer, I. Wechsler, P.G. Marston, M. Mcnallan, High gradient magnetic filtration of steel mill process and waste waters, IEEE Transactions on Magnetics, 11 (1975) 1591-1593.

[83] S. Yiacoumi, C.J. Chin, T.Y. Yin, D.P. Tsouris, D. W., M.R. Chattin, M. Spurrier, Magnetic flocculation and filtration, Office of Scientific & Technical Information Technical Reports, (1996).

[84] J. Wang, J. Yang, H. Zhang, W. Guo, H.-H. Ngo, Feasibility study on magnetic enhanced flocculation for mitigating membrane fouling, Journal of Industrial and Engineering Chemistry, 26 (2015) 37-45.

[85] S.L. Cort, Method and Apparatus for Batch Treating Water Utilizing Magnetic Separation, in, US, 2008.

[86] S.L. Cort, Device and Methods for Shearing Magnetic Floc in a Water Treatment System, in, 2008.

[87] J. Svoboda, Magnetic Separation, in: K.H.J.B.W.C.C.F.I.J.K.M. Veyssière (Ed.) Encyclopedia of Materials: Science and Technology (Second Edition), Elsevier, Oxford, 2005, pp. 1-7.

Table Captions

Table 1 Possible size classification relevant to magnetic separation [18]

Table 2 Charge in frequency Δf with increase in mineral mass [74]

Table 3 The threshold magnetic field B_F (w=1) and a true flocculating magnetic field B^+_F ($t_{1/2}$=1 s) for a suspension containing 10 percent by (volume) of solids [17]

Table 1 Possible size classification relevant to magnetic separation [18]

Particle name	Classification	Size / μm
Coarse	more than	500
Intermediates	less than	500
Fines	less than	100
Very fines	less than	20
Ultrafines	less than	5
Colloids	less than	1
Super colloids	less than	0.2
Nanoparticles	less than	0.02

Table 2 Charge in frequency Δf with increase in mineral mass [74]

Mineral	Particle size / μm	Charge in frequency / Hz
Magnetite	20-45	4000
Hematite	4-8	20
Goethite	0-10	36
Pyrite	20-45	13
Quartz	10-45	4
Pyrrhotite (hexagonal)	20-40	44
Pyrrhotite (monoclinic)	20-45	254

Table 3 The threshold magnetic field B_F (w=1) and a true flocculating magnetic field B^+_F ($t_{1/2}$=1 s) for a suspension containing 10 percent by (volume) of solids [17]

Particle	Hematite		Siderite	
diameter /μm	B_F / T	B^+_F / T	B_F / T	B^+_F / T
1	0.1	0.1	0.45	0.45
5	0.05	0.5	0.23	2.0
10	0.03	3.0	0.12	12.0
20	0.015	10.0	0.05	300.0
40	0.004	20.0	0.017	700.0

Figure Captions

Fig. 1 Magnetic force generated by various magnetic separators, on a hematite particle, as a function of particle size [15].

Fig. 2 Magnetic flocculation in the development of magnetic separation techniques of the current needs [87].

Fig. 3 Schematic representation of the process of magnetic flocculation separation [15].

Fig. 4 Schematic representation of a nanolevel HGMS process consisting of a packed bed with magnetite particles supported on the surface of spherical resin beads [4].

Fig. 5 Coordinate system used in quantifying the interparticle forces $l = r - (a_1 + a_2)$ [8, 28].

Fig. 6 Magnetic-dipole (mag), van der Waals (vdW), and repulsive or attractive electrostatic ($\left|\text{el}\right|$) forces as a function of the dimensionless distance between particle surfaces, for $\varphi = 0$ and different size ratios. Other parameters include $A = 4\times10^{-20}$ J, T = 293 K, $a_l = 5\times10^{-6}$ m, z =1, I = 0.05 M, $\psi_{01} = \left|\psi_{02}\right| = 0.03$ V, B = 5 T, and $\chi_1 = \chi_2 = 0.001$ [28].

Fig. 7 Dimensionless hydrodynamic (viscous) force over a paramagnetic particle with radius (A) R_p=160 nm, or (B) R_p=300 nm for different superficial velocities and as a function of the surface-to-surface separation [4].

Fig. 8 The net inter-particle force (F) vs. distance (D) profiles arising from the summation of several different types of surface-surface interactions. The profiles correspond to (a) strongly attractive, (b) strongly repulsive, and (c) weakly attractive particle-particle interactions. In this representation, negative forces correspond to attraction [44].

Fig. 9 Net dimensionless force between magnetite and a paramagnetic particle under different magnetic fields. Parameters for cases σ_d = 0.01 C/m^2, I = 0.01 N, employs R_s = 400 nm, R_p = 80 nm, and The magnetic susceptibility of the nanoparticle (χ_p), (a) $\chi_p = 2.5\times10^{-4}$, (b) $\chi_p = 2.5\times10^{-3}$ [4].

Fig. 10 Collision efficiencies of particles with various relative sizes and for various values A/(kT) when van der Waals and hydrodynamic forces operate (α=0.1) [51].

Fig. 11 The variation of threshold flocculating magnetic field B_F with particle diameter 2a for assorted minerals. The values of B_F were determined from the total energy curves which at λ =10 reached values in the range (-1 kT, 5 kT) [52].

Fig. 12 Calculated dependence of the stability factor W on the magnetic interaction parameter β for κd = 1. At high fields this relation is a $\beta^{-2/3}$ power law. The various curves correspond to different values of the zero-field stability determined by V_{R0} [2].

Fig. 13 The curves of total potential energy of two hematite particles in the external uniform magnetic field.

The curves were computed for a system described by the following parameters: a =2.5 $\times 10^{-6}$ m; ψ_0 =25 mV; κ= 2.7 $\times 10^{3}$ m^{-1}; χ=2 $\times 10^{2}$ (SI); A =5 $\times 10^{-20}$ J [30].

Fig. 14 Discretization diagram for two initial magnetic-susceptibility classes [59].

Fig. 15 The radius of gyration of a floc chain (R_G) is calculated for each maximum chain cutting off its branches. Blank circles denoting the portion of branches are eliminated from the calculation [63].

Fig. 16 Variation of contained mass as a function of increasing radius, with associated higher fractal dimension [64].

Fig. 17 Freidinger's chart for extrapolation to single floc setting speed and floc building number [70].

Fig. 18 An Eriez Flocculator Magnet (courtesy of Eriez Magnetics, Inc.).

Fig. 19 Generation and growing of aerated flocs inside the FGR [68].

Fig. 20 Device for shearing magnetic floc in a water treatment system [85, 86]

Fig. 1

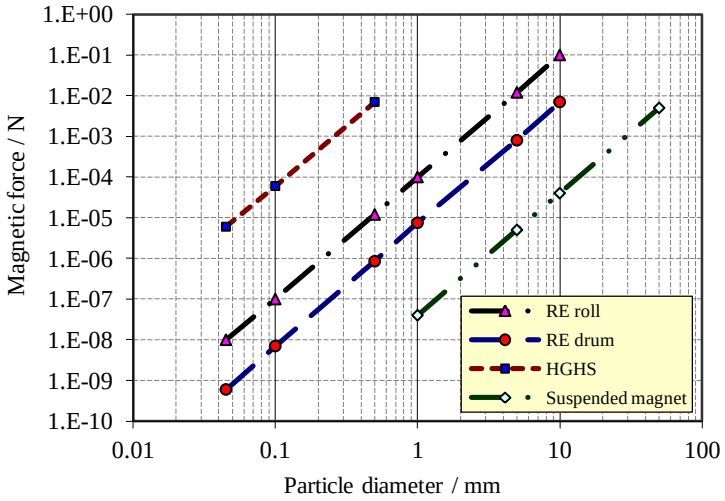

Fig. 2

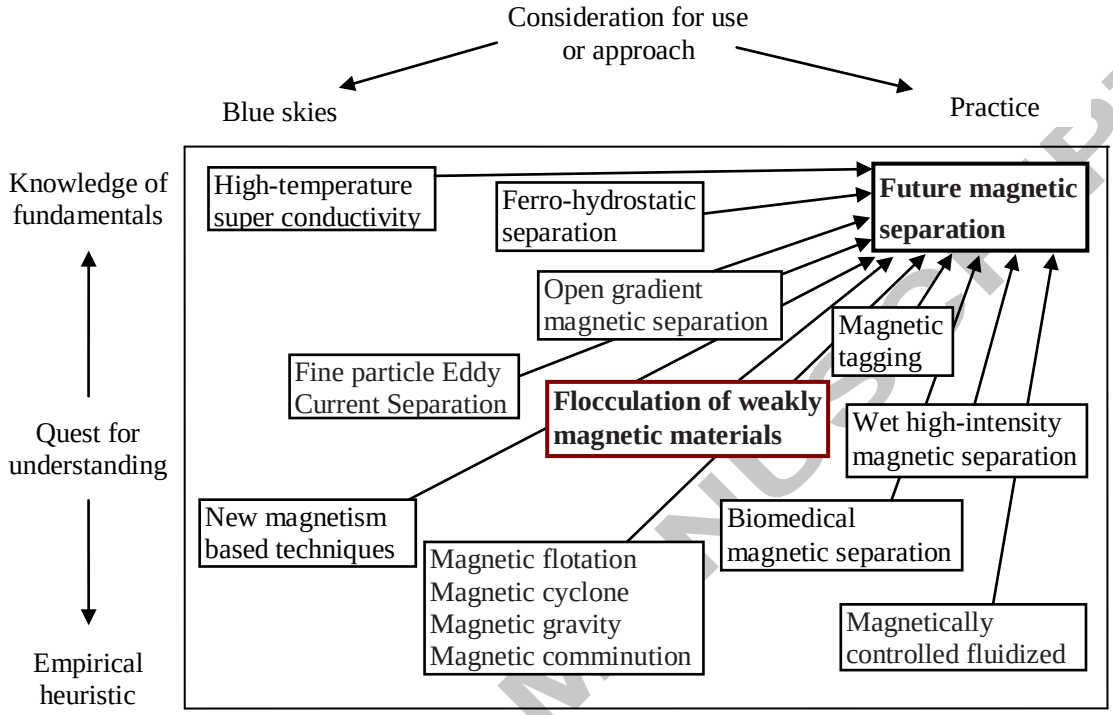

Fig. 3

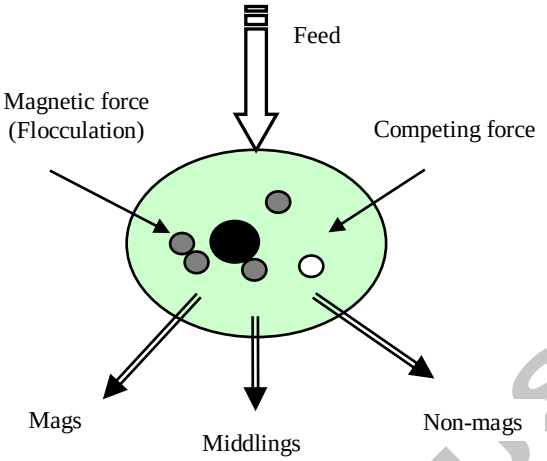

Fig. 4

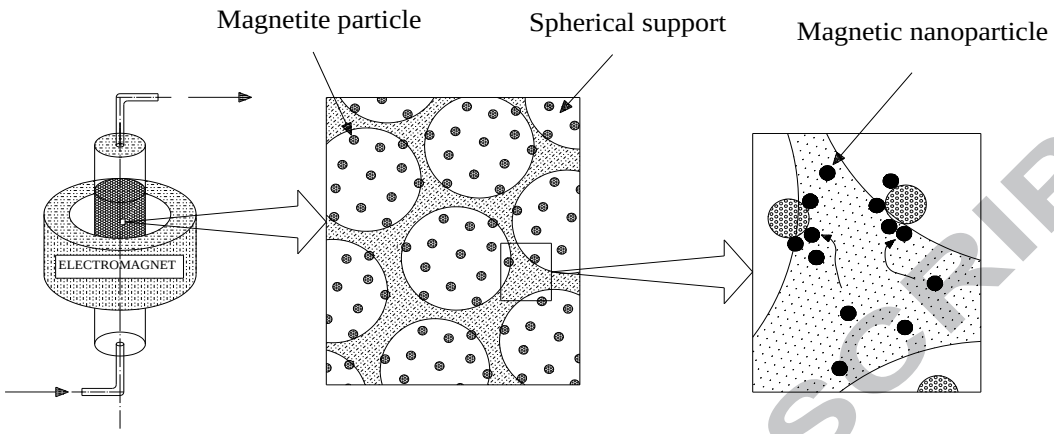

Fig. 5

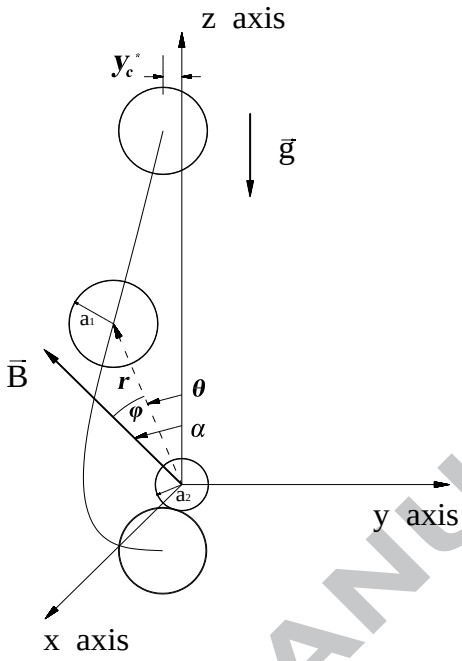

Fig. 6

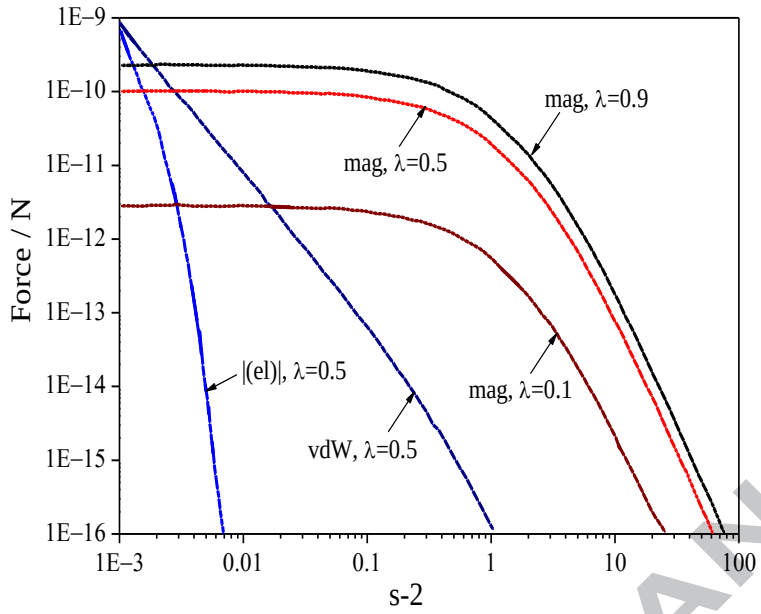

Fig. 7

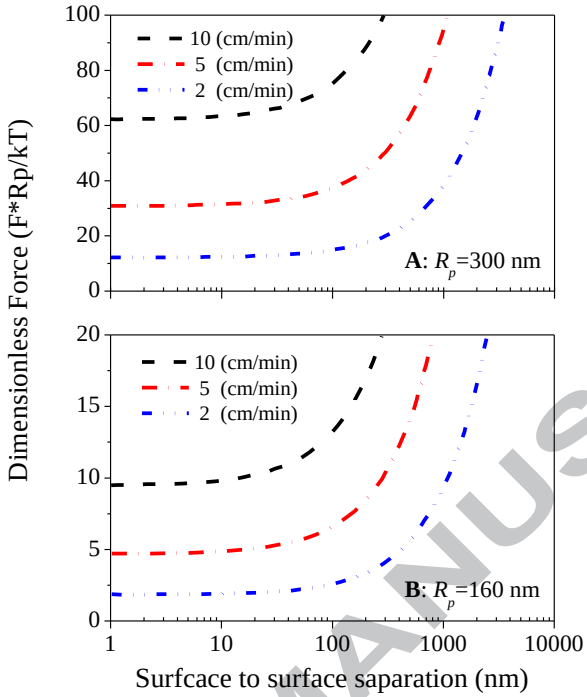

Fig. 8

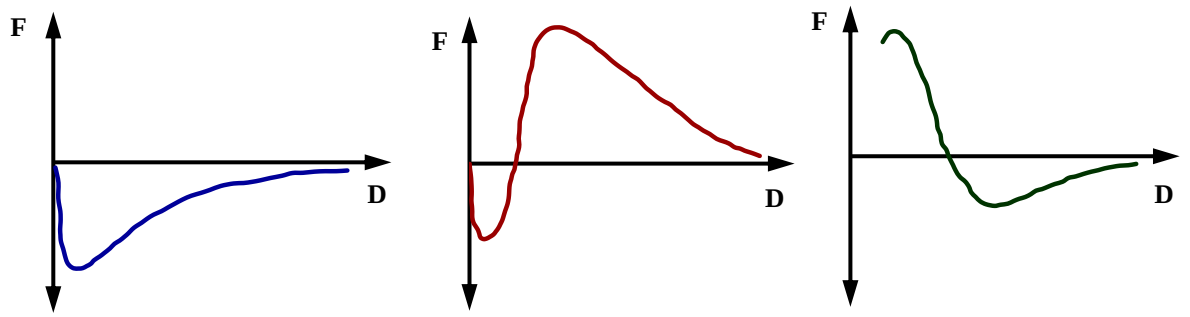

a, strongly attractive **b**, strongly repulsive **c**, weakly attractive

Fig. 9

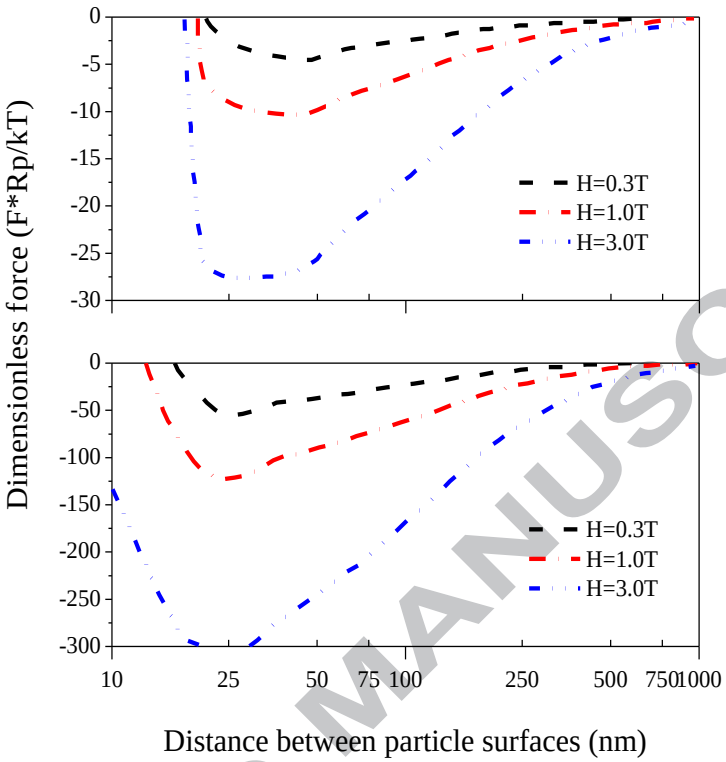

Fig. 10

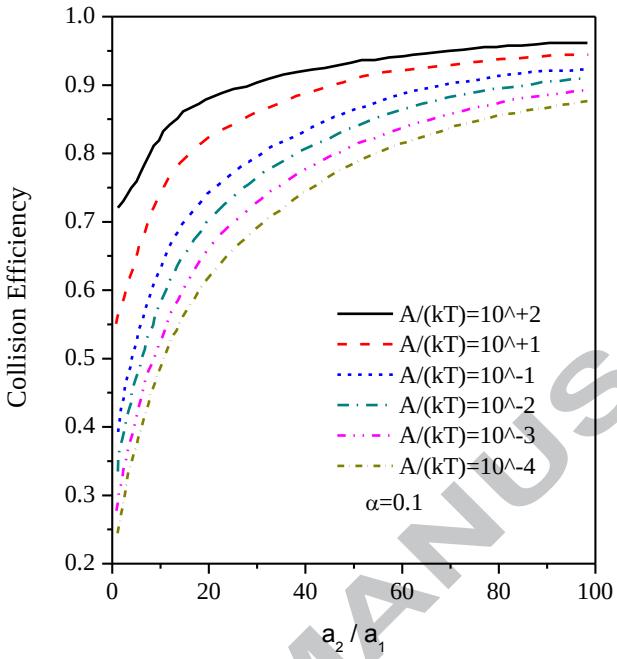

Fig. 11

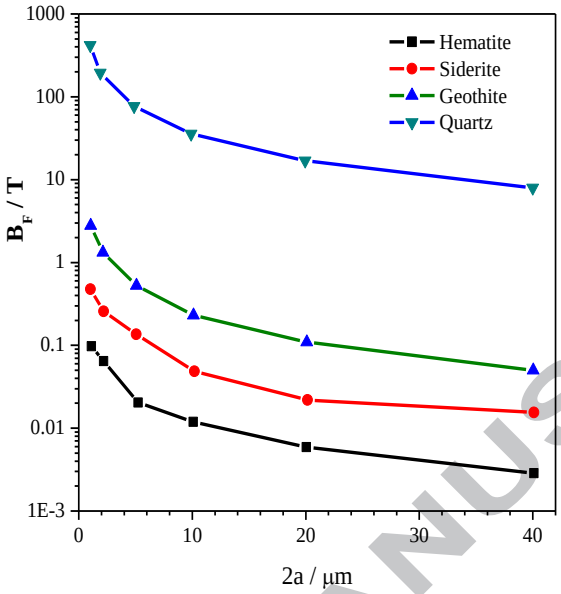

Fig. 12

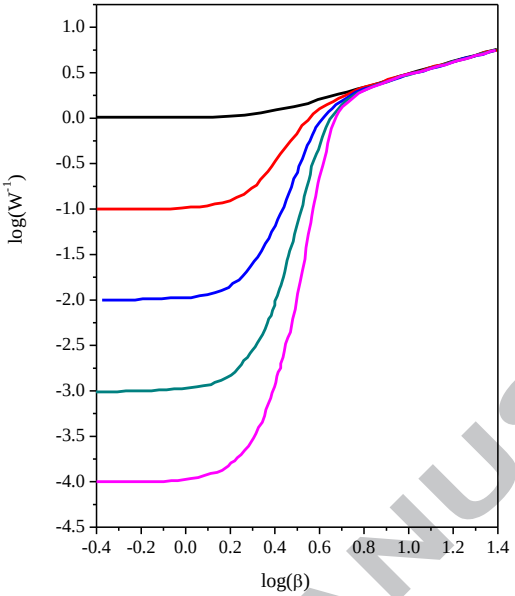

Fig. 13

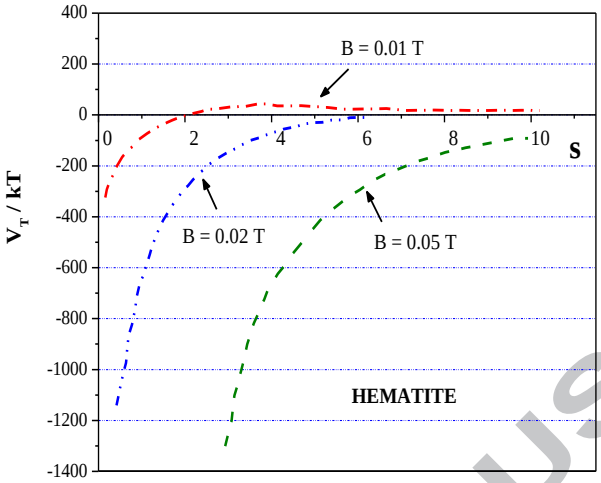

Fig. 14

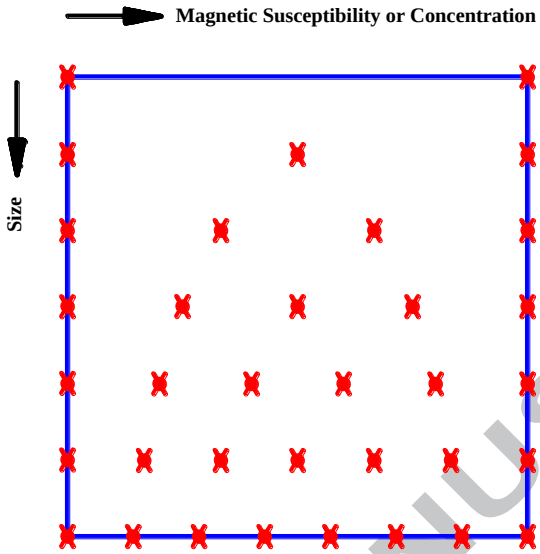

Fig. 15

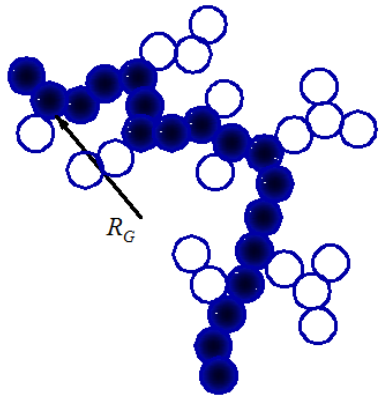

Fig. 16

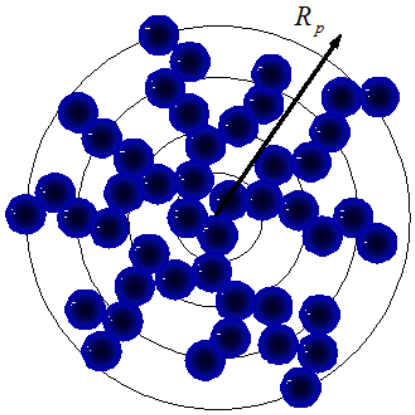

Fig. 17

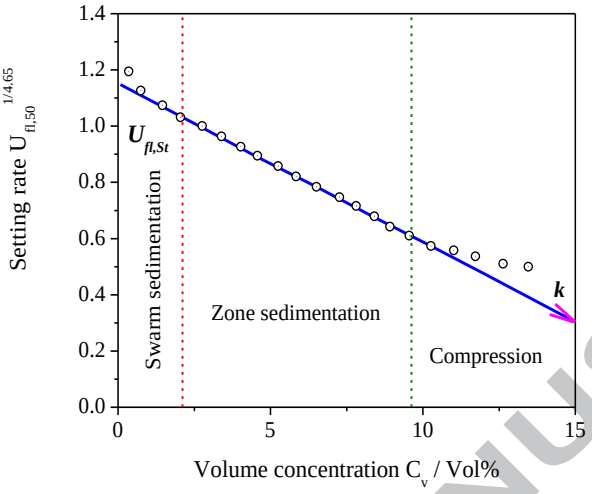

Fig. 18

Fig. 19

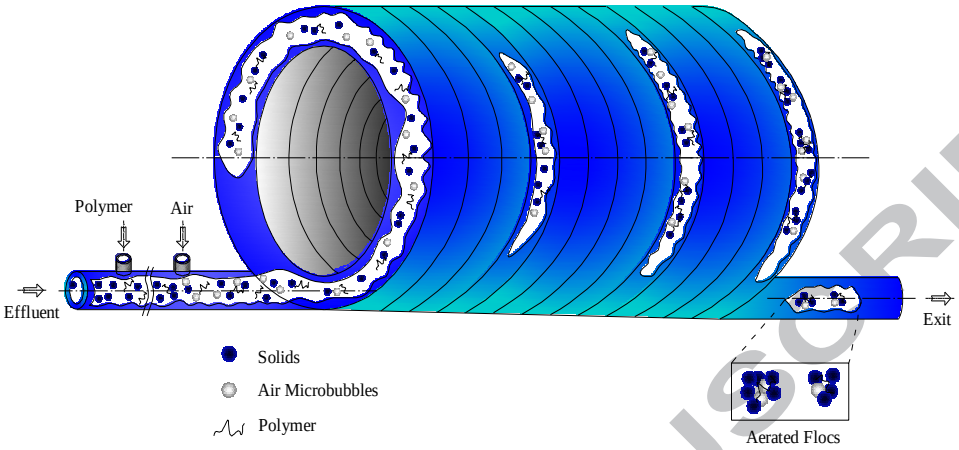

Fig. 20

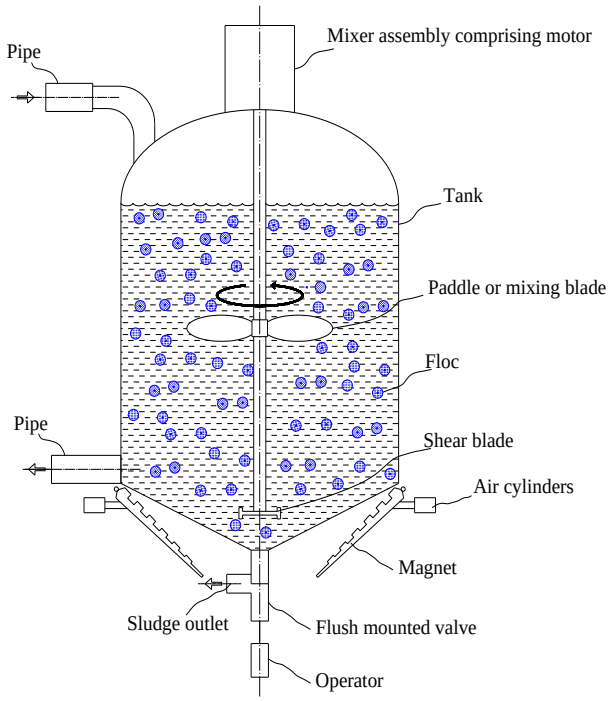

H I G H L I G H T S

- The principles of magnetic separation have been critically reviewed;
- Both external and interparticle forces for ultrafine particles are reviewed and compared;
- Suspensions stability of the particles factors are described and analyzed;
- Various modeling of magnetic flocculation are introduced and some of the applications are illustrated.